Anisotropy Effects on the Plasmonic Response of Nanoparticle Dimers

Alejandro Varas,[†,‡] Pablo García-González,[¶,‡] F. J. García-Vidal,[*,¶] and Angel Rubio[*,§,†,‡]

Nano-Bio Spectroscopy group, Universidad del País Vasco UPV/EHU, CFM CSIC-UPV/EHU-MPC and DIPC, Avenida de Tolosa 72, E-20018 Donostia, Spain, ETSF Scientific Development Centre, Avenida Tolosa 72, E-20018 San Sebastián, Spain, Departamento de Física Teórica de la Materia Condensada and Condensed Matter Physics Center (IFIMAC), Universidad Autónoma de Madrid, E-28049 Cantoblanco, Madrid, Spain, and Max Planck Institute for the Structure and Dynamics of Matter and Center for Free-Electron Laser Science and Department of Physics, Luruper Chaussee 149, 22761 Hamburg, Germany

E-mail: fj.garcia@uam.es; angel.rubio@mpsd.mpg.de

[*]To whom correspondence should be addressed
[†]Nano-Bio Spectroscopy Group, San Sebastián
[‡]ETSF Scientific Development Centre, San Sebastián
[¶]Departamento de Física Teórica de la Materia Condensada and IFIMAC, Universidad Autónoma de Madrid
[§]Max Planck Institute for the Structure and Dynamics of Matter

Abstract

We present an ab-initio study of the anisotropy and atomic relaxation effects on the optical properties of nanoparticle dimers. Special emphasis is put on the hybridization process of localized surface plasmons, the plasmon-mediated photoinduced currents, and the electric-field enhancement in the dimer junction. We show that there is a critical range of separations between the clusters (from 0.1 to 0.5 nm) in which the detailed atomic structure in the junction and the relative orientation of the nanoparticles have to be considered to obtain quantitative predictions for realistic nanoplasmonic devices. It is worth noticing that this regime is characterized by the emergence of electron tunneling as a response to the driven electromagnetic field. The orientation of the particles not only modifies the attainable electric field enhancement but can lead to qualitative changes in the optical absorption spectrum of the system.

Graphical TOC Entry

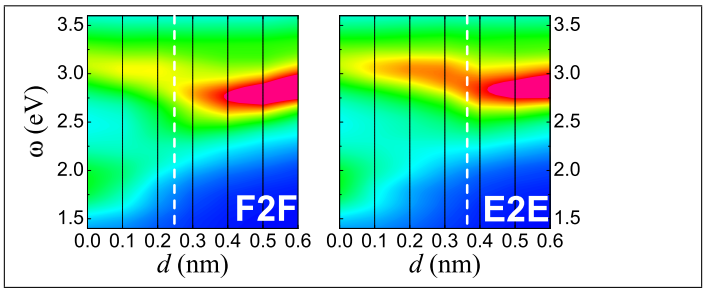

Keywords

Quantum Plasmonics, Ab-initio Methods, Photoinduced Tunneling, Nanoparticle Dimer, Charge-Transfer Modes, Surface-Plasmon Hybridization

The resonant interaction of light with metallic nanostructures is at the heart of the developing field of nanoplasmonics. Recent advances in the fabrication and characterization of nanodevices have opened the possibility of tailoring plasmonic modes and, as a consequence, the response of nanosystems to external radiation.[1–3] Therefore, a number of applications have been realized and/or proposed during the last years: optoelectronic hybrid devices,[4,5] optical nanoantennas,[6] optical traps,[7] nanosensors,[8–10] or broad-band light harvesting devices[11] among others.

Many properties of those nanodevices can be perfectly understood in terms of classical optics.[12] However, if one of the characteristic lengths of the system reaches the sub-nanometric scale, genuine quantum effects emerge in the optical response,[2,13] as have been observed in the last years in a series of breakthrough experiments.[14–18] In this regime, the theoretical treatment of the electromagnetic response must include the inhomogeneities of valence-electron densities and of photoinduced currents between the constituents of the device. Although there are some recent theoretical attemps aiming at incorporating such effects into the realm of classical optics,[19,20] in principle the quantum behavior of both ground-state and light-induced densities should be explicitly treated in order to have reliable theoretical predictions.

A prototypical case is a system made up by two metallic nanoparticles at sub-nanometric separation. In this metallic nanodimer, the establishment of a photoinduced electric current between the particles changes dramatically the plasmonic modes of the system.[21–23] A full account of the main trends[24,25] can be explained by describing the nanoparticles by the spherical jellium model, in which the atomic structure is neglected, and by evaluating the optical response using the, in principle exact, quantum-mechanical time dependent density functional theory (TDDFT).[26–29] The latter provides the necessary accuracy when describing both the inhomogeneity of the electron density and the inherent nonlocality of the electromagnetic response. Hence, the combination of the jellium model and the TDDFT-based quantum treatment of light-matter interactions define what is now considered *state of the art* in theoretical nanoplasmonics. Consequently, this prescription has been applied to analyze the tunable response properties of nanorods,[30] plasmonic cavities formed by nanowires[31–34] and "nanomatryushkas",[35] and more recently the optical properties of doped

semiconductor nanocrystals.[36] Furthermore, the predictions of the jellium/TDDFT method can be also used to assess[31,33] the capabilities of sophisticated refinements of classical optics,[19,20,37–45] whose range of applicability is certainly broader because the numerical implementation of fully quantum methods is limited to systems containing up to thousands of atoms.

The widespread use of the jellium model when analyzing simple *sp* systems can be easily justified on the basis of the collective character of the plasmonic response. Moreover, the dynamical screening due to *d* electrons in noble-metal nanostructures can be mimicked by a dielectric background with an appropriate dielectric function.[46] Then, the atomic structure can be safely neglected in nanostructures made up by weakly-interacting *compact* elements. However, this is not a valid approximation in systems like hybrid nanoclusters,[47] where the chemical composition of the nanoparticle is an essential ingredient to understand its optical properties. Besides, for strongly-coupled nanostructures it has been recently shown that the surface corrugation due to the atomic structure leads to induced near fields with spatial distributions and intensities that are fairly different than the ones obtained from the jellium model.[48] Since, as mentioned before, the electromagnetic response of a nanodimer is greatly affected by the induced current between the particles, it is also expected that the *details* of the atomic arrangement around the dimer junction will have to be taken into account. Thus, a careful analysis is needed in order to quantify the actual role played by the atomic structure in the establishment of induced photocurrents, and determine those regimes in which the detailed description of the atomic geometry is of major relevance. These are the main objectives of the present Letter.

To achieve this goal, we analyze the optical response of a prototype sodium nanocluster dimer. Each cluster is made up by 297 atoms in an icosahedral arrangement, which is the most stable configuration for isolated Na nanoparticles of this size.[49,50] As can be seen in Figure 1, the Na_{297} cluster is almost spherical, being $2R \simeq 2.61$ nm its effective diameter. This value corresponds to an averaged atomic density which is slighty larger than the one corresponding to bulk Na. The distance between the clusters is defined as $d = b - 2R$, where b is the distance between the central atoms of each cluster. Therefore, this definition does not depend on any atomic rearrangement in

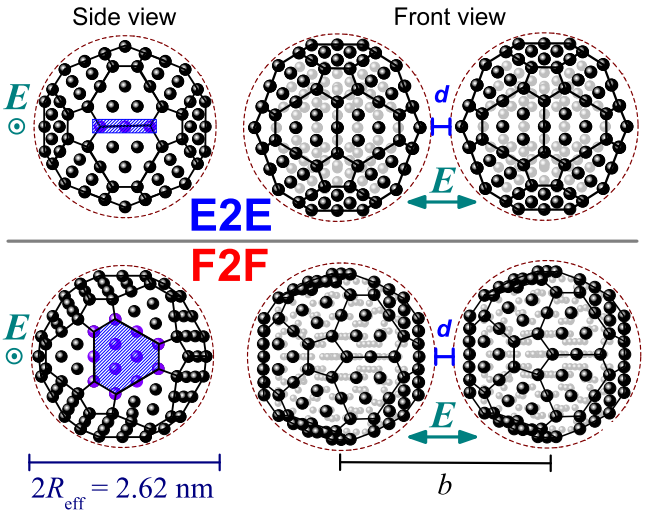

Figure 1: Representation of the two different geometrical arrangements of icosahedral Na_{297} dimers considered in the present work. In the edge-to-edge (E2E) relative orientation (upper panel), two 3-atom edges are faced. In the face-to-face (F2F) relative orientation (lower panel), the spacial gap is between two 12-atom faces. The applied electric field is orientated along the dimer axis.

the gap region.

Once the distance d is fixed, there are two main features to consider: the relative orientation of the clusters and the atomic relaxation due to the mutual interaction. Concerning the relative orientation, in the present work we treat the two cases depicted in Figure 1. The first one leads to a spatial gap which is limited by two 12-atom faces (F2F orientation), whereas the second one corresponds to a spatial gap between two 3-atom edges (E2E orientation). Thus, in the F2F geometry we maximize the width of the dimer junction whereas the E2E configuration corresponds to a smaller separation between atoms. That is, there are two distinct effects (the distance between the nearest-neighbors atoms and the contact width) which tend to cancel out. Besides, we perform an energy-optimized relaxation of the atomic positions in the E2E geometry, which is required due to the smaller distance between atoms. Of course, such a relaxation has to be restricted to the region around the spacial gap, since the dimer itself is metastable: the full relaxation would lead to the coalescence of the two clusters.

Both energy optimization and ground-state calculations are performed under a real-space prescription of the density functional theory (DFT) Kohn-Sham equations[51] using the OCTOPUS

package.[52–55] The explicit treatment of the $3s$ conduction electrons by using norm-conserving pseudopotentials[56] suffices for the purposes of the present work. The relaxation is performed using the FIRE algorithm,[57] recently implemented in OCTOPUS,[55] under a semilocal approximation to the exchange-correlation (XC) functional. Once the equilibrium geometries have been obtained, ground-state electron densities, $n_0(\mathbf{r})$, are evaluated using the same prescription.

The TDDFT optical response is also calculated with OCTOPUS following the Yabana-Bertsch time-propagation recipe,[58] which is very efficient in systems containing hundreds of atoms. At $t = 0$ the electron system is perturbed by a delta-kick electric field $\mathbf{E}(\mathbf{r},t) = (\hbar\kappa_0/e)\delta(t)\mathbf{e}_x$, where e is the absolute value of the electron charge, $\mathbf{e}_x$ is the direction of the dimer axis (i.e., the external field is oriented along the dimer junction), and $\kappa_0 = 0.005$a.u.. Then, all the E1 selection-rule transitions are excited, and the induced density of a transition of frequency ω is directly related to the time-dependent density of the system after the kick, $n(\mathbf{r},t)$, though a Fourier transform:

$$\delta n(\mathbf{r},\omega) = \int_0^\infty \delta n(\mathbf{r},t) e^{(i\omega-\gamma)t} \simeq \int_0^{T_{\max}} \delta n(\mathbf{r},t) e^{(i\omega-\gamma)t} dt \ , \tag{1}$$

where $\delta n(\mathbf{r},t) = n(\mathbf{r},t) - n_0(\mathbf{r})$. Here, $\gamma = 0.1$ eV$/\hbar$ is a damping frequency which accounts for absorption spectra broadening due to non-electronic losses and $T_{\max}$ is the actual propagation time in the calculations. The absortion cross-section is then given by $\sigma_{\rm abs}(\omega) = (\omega/c\varepsilon_0)\mathrm{Im}\alpha(\omega)$, where the dynamical polarizability $\alpha(\omega)$ is

$$\alpha(\omega) = -\frac{e^2}{\hbar\kappa_0}\int x\delta n(\mathbf{r},\omega) d\mathbf{r} \ . \tag{2}$$

In practice, $\alpha(\omega)$ is evaluated from the Fourier transform of the kick-induced time-dependent dipole moment. Well-converged results are achieved using $T_{\max} = 20$fs, a propagation-time step $\Delta t = 10^{-4} T_{\max}$, and a grid spacing of 0.026 nm.

The dipole optical absorption of Na_{297} dimers in the range of separations $0 \leq d \leq 0.6$ nm is presented in Figure 2 for the unrelaxed F2F and the relaxed E2E geometries. For completeness, we have also included the optical absorption for the E2E overlapping clusters ($d = -0.1$ nm), where a

major reconstruction of the junction occurs. We can define three distinct regimes: (a) $d \geq 0.6$ nm, where the interaction between clusters is mainly electromagnetic and the photoinduced charge transfer (CT) is very small; (b) $d \leq 0.1$ nm, where there is a direct overlap of the ground-state densities of each cluster because the Fermi level of the system is above the potential barrier in the dimer junction; and (c) 0.1 nm $< d <$ 0.6 nm where tunnelling CT between the clusters appears as a result of a photoinduced voltage bias between the clusters.

As can be seen in Figure 2, there are marginal differences between the E2E and F2F optical spectra for the separation regimes (a) and (b). The irrelevance of the relative orientation of the clusters in the regime (a) is not a surprise at all since there are minor differences between the F2F absorption and the spherical jellium model one even when $d = 0.5$ nm.[48] Furthermore, this is the regime where the optical absorption can be well explained in classical terms, being also possible a quantitative agreement with the quantum predictions as long as the nonlocality of the electromagnetic response and the inhomogeneity associated to the electron-density spill-out in each nanoparticle were properly addressed. As it is well known,[21,39,59–61] the optical absorption in this regime is dominated by the coupling between the Mie dipole localized surface plasmon resonances (LSPRs) of the individual clusters. This coupled mode, in what follows labelled as D, is redshifted with respect to the value $\omega_{\mathrm{M}} = 3.13\ \mathrm{eV}/\hbar$ of the main Mie resonance of the isolated Na_{297} cluster.[48] In addition, a weak but discernable spectral feature appears at higher frequency. This is the signature of a hybridized plasmon resonance (Q) due to the excitation of the quadrupole LSPR of each cluster by the induced near field of the other.

As mentioned above, the regime (b) corresponds to direct overlapping of ground-state densities. In this limit, the two clusters cannot be consider as individual entities anymore and the system is actually a single ”peanut-like” nanoparticle. The atomic arrangements in the junction and at the surfaces are very different in the F2F and E2E geometries, but such differences are blurred in the valence-electron density. As a consequence, the classically-predicted sensitivity of the propagation of surface modes with respect to the surface inhomogeneities[62] is not longer relevant. In this case, the spectrum is dominated by two LSPRs, labelled as D(CT) and Q(CT). In both resonances, there

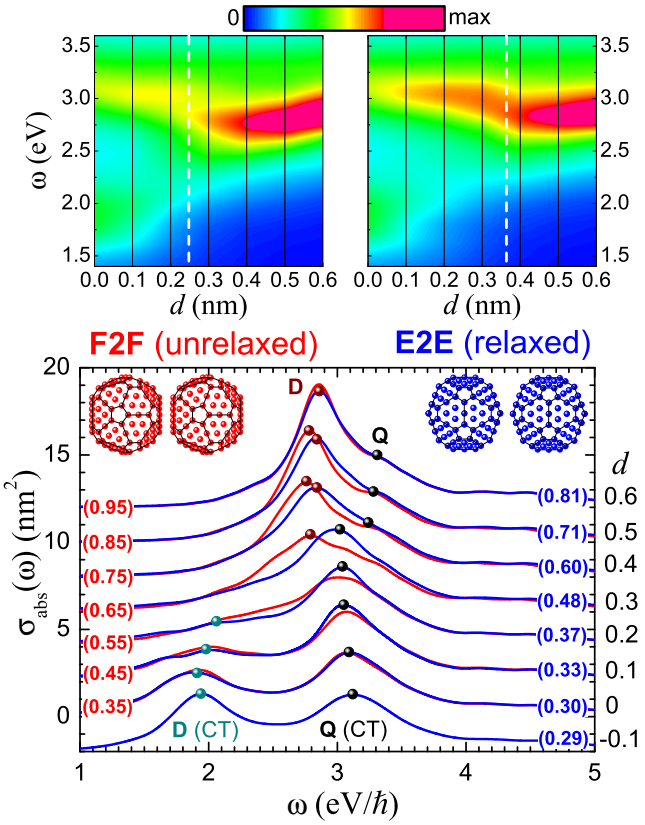

Figure 2: Optical absorption of Na_{297} dimers vs the distance d as defined in the text. Upper panels: contour plots of the photoabsorption cross sections, $\sigma_{\rm abs}(\omega)$. The vertical dashed line indicates the approximate distance where the hybridized Q mode becomes the main spectral feature in the spectrum. Lower panel: waterfall plot of the absorption cross sections. The red [blue] lines correspond to the F2F [relaxed E2E] relative orientations. For each distance, the separation in nm between faces [edges] is indicated between parenthesis. The spectral peaks corresponding to coupled D, charge-transfer D and Q, and hybridized Q modes are indicated as well.

is a capacitive charge transfer between the two clusters (actually, between the two lobes of the peanut-shaped nanoparticle). In turn, these modes can be also characterized using classical optics if the actual ground-state density of the system is properly modeled.[61,63]

On the contrary, the importance of the atomic structure is clearly manifested in the regime (c), where the optical absorption of the dimer is the result of a delicate interplay of the electromagnetic interaction mediated by near fields and the appearance of a tunelling CT between the clusters. When $d \geq 0.4$ nm, the splitting of the D and Q modes in the F2F geometry is clearly visible. Furthermore, the frequency of the D mode decreases when approaching the clusters. Thus, the

behavior of the F2F response can be described by classical electromagnetism, despite the fact that there is a charge transfer between the clusters as we will show below. For the other geometry, E2E, the value of the frequency of the D mode is already locked in this range of separations and the transfer of spectral weight from the D mode to the hybridized Q mode is clearly reflected on the spectrum. Interestingly, the intensity of the tunneling current, I_{CT}, when the D mode is excited is very similar in the F2F and E2E configurations. However, since the junction in the E2E orientation is substantially narrower than in the F2F one, the CT *current density* across the spatial gap is greater in the E2E case. As a consequence, the propagation of the plasmonic density waves over the surface of the clusters is slightly altered by the tunneling CT in the F2F geometry, and the hybridization process follows the classically-predicted trends. In fact, the quantum effects are only discernible in the F2F spectrum when the distance d is less than 0.4 nm. However, the E2E optical response is much more sensitive to the establishment of an induced current, and we can say that the onset of quantum behavior due to tunneling is above $d = 0.5$ nm.

Within the regime (c), the differences are more dramatic at smaller separations. In the F2F orientation at $d = 0.3$ nm, the D mode still dominates the spectrum, but the corresponding mode in the E2E geometry has been already quenched and the main spectral feature comes from the hybridized Q mode. Nevertheless, this interpretation cannot be taken literally since, unlike the well-defined classical plasmon modes, quantum collective excitations are the result of a coherent superposition of multiple electron-hole transitions which, besides, cannot be isolated from other surrounding electron-hole pairs. In fact, the broad absorption range that characterizes both spectra at $d = 0.3$ nm is an admixture of the quantum collective excitations corresponding to the classical D and Q modes, electron-hole transitions, and likely other many-body collective excitations.[64] In any case, at $d = 0.3$ nm the two spectra are *qualitatively* different, and such a difference will be even more evident when analyzing the driven induced densities and currents. The spectral feature corresponding to the D mode in the F2F orientation finally vanishes when the separation is smaller than 0.3 nm, and the maximum absorption at $d = 0.2$ nm corresponds to the excitation of a Q mode for both geometries. Note that there is still a reminiscence of the D mode excitation in the F2F

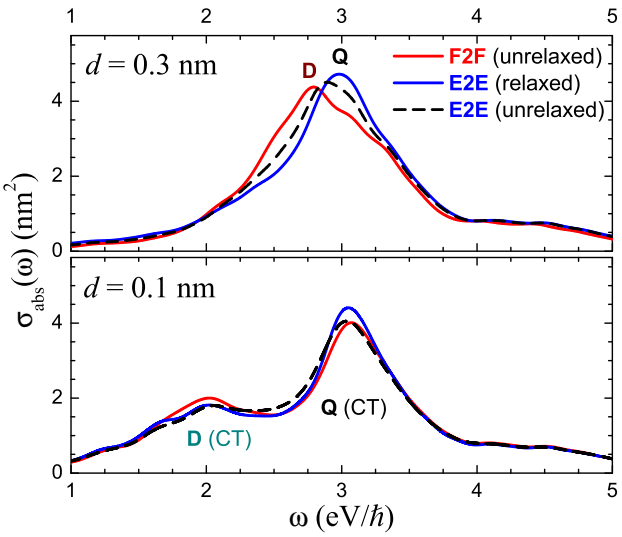

Figure 3: The impact of the atomic relaxation on the absorption cross sections for E2E Na_{297} dimers at separations $d = 0.1$ nm and $d = 0.3$ nm. Optical absorption for relaxed geometries: solid blue lines; absorption for unrelaxed geometries: dashed lines. For the sake of comparsion, the corresponding F2F spectra are also depicted (red solid lines).

spectrum, around $\omega = 2.3$ eV$/\hbar$.

Let us now analyze the impact of the atomic relaxation in the optical absorption. The corresponding reconstruction in the junction is negligible if the distance between nearest-neighbour atoms is greater than 0.6 nm, and hardly noticeable in the range $0.5 - 0.6$ nm. That means that relaxation effects are expected to be significant if $d \lesssim 0.4$ nm for the E2E geometry and if $d \lesssim 0.25$ nm for the F2F configuration. For shorter distances, when the atomic densities of both clusters overlap, the atomic reconstruction itself will be noticeable. However, we have seen that in this regime the specific atomic arrangement is not a fundamental issue. Therefore, the atomic relaxation will play a role only in the range of critical distances where there is a transition from a dominant D mode to a Q mode. To confirm and quantify this prediction, we compare the relaxed-E2E optical absorption considered so far with the unrelaxed-E2E one at $d = 0.3$ nm and $d = 0.1$ nm. Such a comparison is depicted in Figure 3 where, as expected, we may see that the atomic relaxation has a marginal impact in the optical response when $d = 0.1$ nm. At the critical distance $d = 0.3$ nm, the separation between the atoms is slightly greater in the unrelaxed configuration

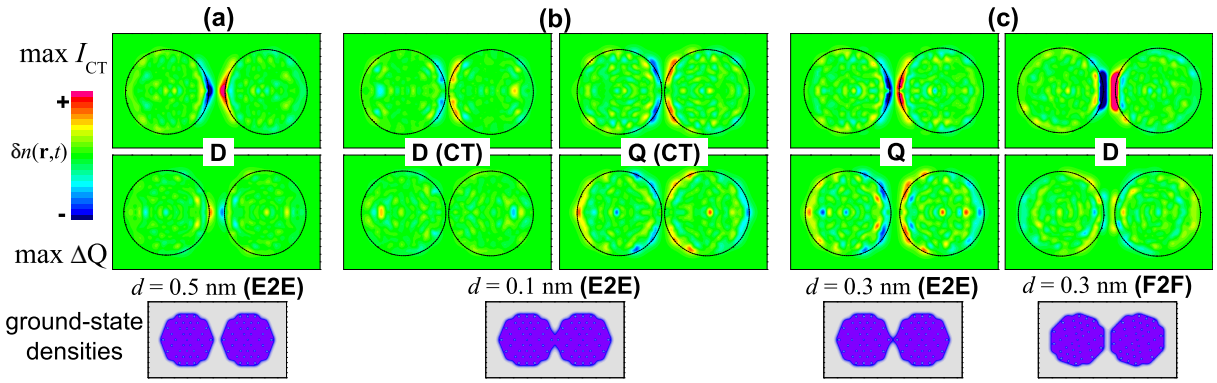

Figure 4: Snapshots of the induced electron densities at different resonant frequencies, as indicated in each panel. The top panels depicts the induced densties when the current between clusters reaches a maximum, wheras the second line corresponds to induced densties when the charge difference between clusters is maximum (zero intensity). The scale range is $-\rho \leq \delta n \leq +\rho$, where $\rho = 0.5 \times 10^{-6}$ a.u. for $d = 0.1$ nm and $d = 0.3$ nm, whereas $\rho = 10^{-6}$ a.u. for $d = 0.5$ nm. A sketch of the corresponding ground-state electron densities is also shown to illustrate the different contact regimes.

than in the relaxed one (0.51 nm and 0.48 nm, respectively). This small rearrangement does affect the absorption spectrum because the intensity of the tunneling CT is weaker in the unrelaxed configuration. In any case, the changes are merely quantitative and less important than those related to the relative orientation, albeit illustrating the extreme sensitivety of the plasmonic response to the CT current intensity.

To get further insights concerning the optical properties of the nanocluster dimers, we analyze the electron dynamics at different resonant frequencies. Specifically, we look at the induced densities, the current intensities between the clusters, and the total electric field (external plus induced) at the middle of the junction, $\mathbf{r} = \mathbf{0}$. To carry out this study, we apply over the system a weak uniform quasi-monochromatic laser pulse of mean frequency ω_{ext} and duration $\tau = 20\pi/\omega_{\rm ext}$ given by

$$\mathbf{E}(t) = -E_0 \sin(\pi t/\tau)\cos(\omega_{\rm ext} t)\mathbf{e}_x \,, \tag{3}$$

where $E_0 = 10^{-6}$ a.u. $\simeq 0.51 \times 10^6$ V m^{-1} is the maximum amplitude of the incident electric field. The maximum intensity of the laser pulse is 34.5 kW cm^{-2}, well below the onset of nonlinear effects.[25]

In Figure 4 we depict snapshots of the photoinduced densities in a plane containing the dimer axis for the following selected cases: a) D mode at $d = 0.5$ nm (E2E, $\omega_{\text{ext}} = 2.83$ eV$/\hbar$); b) D and Q modes at $d = 0.1$ nm (E2E, $\omega_{\text{ext}} = 2.01$ eV$/\hbar$ and $\omega_{\text{ext}} = 3.05$ eV$/\hbar$, respectively); c) D mode (F2F, $\omega_{\text{ext}} = 2.79$ eV$/\hbar$) and Q mode (E2E, $\omega_{\text{ext}} = 3.00$ eV$/\hbar$) at $d = 0.3$ nm. In all the cases, the relaxed atomic geometries were used for the E2E relative orientation. The snapshots are collected at times where the induced current is maximum (i.e., when the two clusters have the same charge) and where the induced current is close to a minimum (i.e., when the net charge of each cluster reaches its maximum absolute value).

Case a) is representative of a coupled D mode (albeit very slightly altered by the appearance of a tunneling CT). The coupling between the dipole resonances of each cluster is reflected by a high concentration of oscillating induced charges of opposite sign in the sides of the junction. As it has been extensively analyzed using classical and quantum prescriptions, this distribution of charge is the primary reason of the high electric field enhancements that appears in this plasmonic cavity.

In case b) we show direct-CT modes. Although the overall shape of the driven densities are partially obscured by the atomic corrugation, the different nature of the D and Q modes is evident. Also note that the induced densities are practically zero in the junction, in fair correspondence with the single-nanoparticle character of the system at this separation.

Finally, case c) illustrates the sensitivity of the dynamical response to the atomic configuration in the critical regime in which the optical absorption is dramatically affected by the photoinduced electron tunneling. The most relevant aspect is the difference between the E2E and F2F driven densities. The first can be assigned to a Q mode (compare with the corresponding Q mode at 0.1 nm), whereas the second has a shape closer to a D mode. Also note the different distributions of the induced densities around the spacial gap between the clusters.

In Figure 5 we display the time-evolution of the induced current, I_{CT}, and the total electric field at the middle of the junction ($\mathbf{r} = \mathbf{0}$) for the three cases discussed above. We have also included the induced current and field for the F2F configuration at $d = 0.5$ nm (D mode, $\omega_{\text{ext}} = 2.78$ eV$/\hbar$). It is worth emphasizing the overall delay in the response with respect to the applied field and the

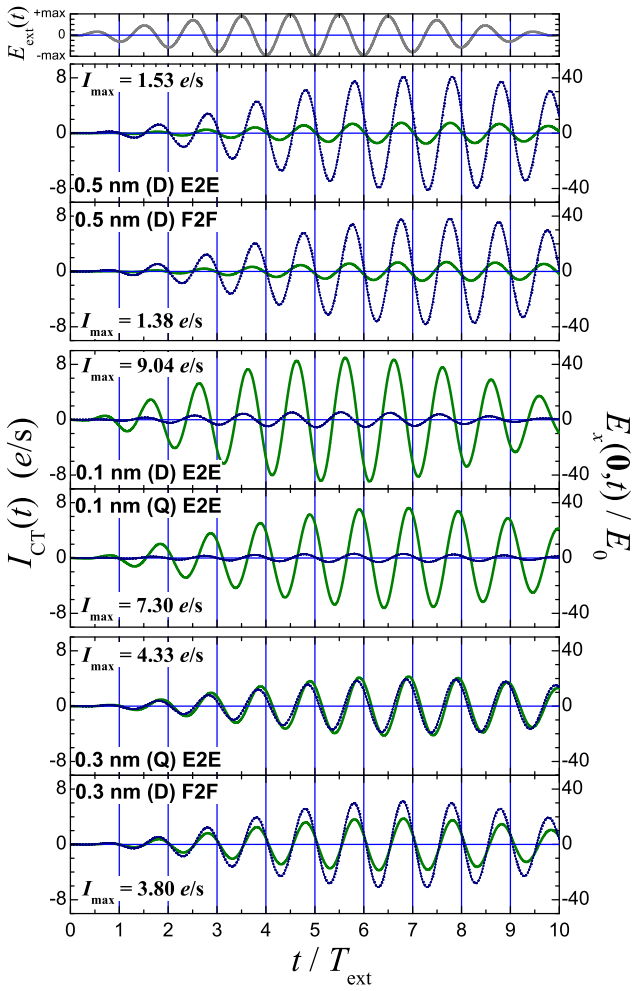

Figure 5: Time evolution of induced currents (solid green lines) and total electric fields (dotted blue lines) at the middle of the dimer junction ($\mathbf{r} = \mathbf{0}$) due to the resonant coupling of selected modes of the nanoparticle dimer with an applied external field (depicted in the upper panel) of frequency ω_{ext}. In each panel we indicate the maximum value of the induced intensity, I_{CT}.

persistence of the induced currents and fields even when the external field has vanished, obvious signatures of a resonant coupling. Non-electronic loses are not included in this calculation and, therefore, the decay of the driven modes can only occur via Landau fragmentation, i.e, though formation of electron-hole pairs.[65,66] In any case, the excitation of electron-hole pairs is the main damping mechanism of plasmons in nanoparticles of this size. Note that the generation of hot electrons after the plasmon decay is a very efficient mechanism that has important implications, for instance, in heterogeneous catalysis.[67]

The electric fields at $\mathbf{r} = \mathbf{0}$ for the two coupled D modes at $d = 0.5$ nm here considered (EFE and F2F) are very similar, although the field corresponding to the E2E geometry is slightly more intense. We can attribute this effect to the shorter atom-atom distance and also to the more angular profile of the induced density in the E2E configuration. On the other hand, fields and intensities practically oscillates in phase, as corresponds to a resistive character of the junction. This behavior agrees with the obtained for jellium nanocluster[25] and nanowire dimers.[33] Note the weak charge-transfer intensity (of the order of 1.5 *e*/s, where *e* is the absolute value of the electron charge) for the incidente laser pulse given in Eq. (3).

Focusing on the direct CT regime, $d = 0.1$ nm, first of all we must note the different phase shifts of the oscillations of both the Q and D modes with respect to the applied field. Moreover, for both resonances, there is a relative phase between the induced current and the electric field in the center of the dimer, the intensity being delayed with respect to the total electric field. Again, this capacitive character of the resonance is in full agreement with the previous findings for jellium systems.[25,33] Although the optical absorption at the D mode is weaker than at the Q resonance (see Figure 1), the E-field intensity is stronger in the D mode. Nevertheless, once the applied field fades out, the amplitudes of the D mode oscillations are quickly damped as expected from the wider corresponding peak in the absorption spectrum. Finally, in this regime the charge-transfer intensity is about one order of magnitud larger than in the tunneling regime previously described (at touching distance, $d = 0$, the maximum charge-transfer intensity is 17.0 *e*/s).

In line with the previous discussion, there are substantial differences between the E2E and F2F orientations in the intermediate-distance regime, $d = 0.3$ nm. The intensities of the driven currents are rather similar, up to a small relative phase. However, the electric field in the E2E geometry is weaker than in the F2F orientation. This is not surprising because the dominant mode in the E2E geometry is the Q resonance. Remarkably, the intensity and the total E-field oscillate in phase in the F2F dimer, thus indicating that the charge flows across a resistive junction. On the contrary, the E field and the current do not oscillate completely in phase in the E2E geometry. This is consistent with a weak capacitive behavior, which again can be traced back to the different atomic

configurations in the junction.

Summarizing, in this Letter we have presented a detailed study of the impact of the atomic configuration on the electromagnetic modes of prototypical metallic nanodimers when a charge transfer is established between the constituent clusters. Effects like atomic relaxation and different relative orientations, so far unexplored in quantum implementations of ab-initio nanoplasmonics, have been explicitly addressed. Our findings confirm the accuracy of the jellium model, either combined with quantum mechanical calculations or classical theories, except in the sub-nanometric separation regime in which the photoinduced tunnel current leads to dramatic changes in the optical properties of the system. This is precisely the regime where the most complicated processes occur. Thus, we have shown that a full account of the atomic structure of the junction between closed nanoparticles is mandatory to obtain theoretical results with enough predicitive power.

Although quantum TDDFT simulations can be applied to systems containing thousands of atoms, this is still below the sizes of many nanoparticles of technological interest. Then, the theoretical analyses aimed at helping the design and characterization of novel nanodevices must be necessarily done by using either advanced prescriptions of the well-stablished classical electromagnetic theory [19,20] or simplified TDDFT methods. [68,69] However, even in simple systems like the one analyzed in this work, there is a subtle interplay between induced near fields (which can be perfectly described classically using non-local optics) and induced tunnel charge transfers (which can be *approximately* accounted for using effective dielectric media [20]). Therefore, the present work provides an stringent playfield for the assessment of future refinements of semiclassical theories which, as we have mentioned, are much more amenable for the analysis of very complex structures than quantum ab-initio methods. From a different perspective, the conclusions raised in this Letter also paves the way to further explorations concerning fields like optoelectronics, nanosensing, or photoinduced catalysis where the complexity of the light-matter interaction at the nanoscale opens the possibility of a panoply of applications.

Acknowledgement

We thankfully acknowledge the financial support by the European Research Council (ERC-2010-AdG Proposal No. 267374 and ERC-2011-AdG Proposal No. 290891), the Spanish Government (grants MAT2011-28581-C02-01, FIS2013-46159-C3-1-P, MAT2014-53432-C5-5-R), and the Basque Country Government (Grupos Consolidados IT-578-13). We also appreciate the technical support by Joseba Alberdi-Rodríguez and fruitful discussions with Prof. Javier Aizpurua, Prof. Juan Carlos Cuevas, Dr. Johannes Feist, Dr. Antonio Fernández-Domínguez, and Dr. Pu Zhang.

References

(1) Schuller J. A.; Barnard E. S.; Cai W., Jun Y. C.; White J. S.; and Brongersma M. L. Plasmonics for extreme light concentration and manipulation. *Nature Materials* **2010**, *9*, 193-204.

(2) Halas, N. J.; Lal, S.; Chang, W.-S.; Link, S.; Nordlander, P. Plasmons in Strongly Coupled Metallic Nanostructures. *Chem. Rev.* **2011**, *111*, 3913-3961.

(3) Gray, S. K. Theory and Modeling of Plasmonic Structures. *J. Phys. Chem. C* **2013**, *117*, 1983-1994.

(4) Ward, D. R.; Hüser, F.; Pauly, F.; Cuevas, J. C.; Natelson, D. Optical Rectification and Field Enhancement in a Plasmonic Nanogap. *Nature Nanotechnology* **2010**, *5*, 732-736.

(5) Galperin, M.; Nitzan, A. Molecular optoelectronics: the interaction of molecular conduction junctions with light. *Phys. Chem. Chem. Phys.* **2012**, *14*, 9421-9438.

(6) Mühlschlegel, P.; Eisler, H.-J.; Martin, O. J. F.; Hecht, B.; Pohl, D. W. Resonant Optical Antennas. *Science* **2005**, *308*, 1607-1609.

(7) Tsuboi, Y.; Shoji, T.; Kitamura, N.; Takase, M.; Murakoshi, K.; Mizumoto, Y.; Ishihara, H. Optical Trapping of Quantum Dots Based on Gap-Mode-Excitation of Localized Surface Plasmon. *J. Phys. Chem. Lett.* **2010**, *1*, 2327-2333.

(8) Xu, H.; Bjeneld, E. J.; Käll, M.; Börjesson, L. Spectroscopy of Single Hemoglobin Molecules by Surface Enhanced Raman Scattering. *Phys. Rev. Lett.* **1999**, *83*, 4357-4360.

(9) Stewart, M. E.; Anderton, C. R.; Thompson, L. B.; Maria, J.; Gray, S. K.; Rogers, J. A.; Nuzzo, R. G. Nanostructured Plasmonic Sensors. *Chem. Rev.* **2008**, *108*, 494-521.

(10) Vo-Dinh, T.; Dhawan, A.; Norton, S. J.; Khoury, C. G.; Wang, H.-N.; Misra, V.; Gerhold, M. D. Plasmonic Nanoparticles and Nanowires: Design, Fabrication and Application in Sensing. *J. Phys. Chem. C* **2010**, *114*, 7480-7488.

(11) Aubry, A.; Lei, D. Y.; Fernández-Domínguez, A. I.; Sonnefraud, Y.; Maier, S. A.; Pendry, J. B. Plasmonic Light-Harvesting Devices over the Whole Visible Spectrum. *Nano Lett.* **2010**, *10*, 2574-2579.

(12) Maier, S. A. *Plasmonics: Fundamentals and Applications*; Springer: New York, **2007**.

(13) Tame, M. S.; McEnery, K. R.; Özdemir, S. K.; Lee, J.; Maier, S. A.; Kim, M. S. Quantum Plasmonics. *Nature Physics* **2013**, *9*, 329-340.

(14) Arielly, R.; Ofarim, A.; Noy, G.; Selzer, Y. Accurate Determination of Plasmonic Fields in Molecular Junctions by Current Rectification at Optical Frequencies. *Nano Lett.* **2011**, *11*, 2968-2972.

(15) Savage, K. J.; Hawkeye, M. M.; Esteban, R.; Borisov, A. G.; Aizpurua, J.; Baumberg, J. J. Revealing the Quantum Regime in Tunneling Plasmonics. *Nature* **2012**, *491*, 574-577.

(16) Scholl, J. A.; García-Etxarri, A.; Koh, A. L.; Dionne, J. A. Observation of Quantum Tunneling between Two Plasmonic Nanoparticles. *Nano Lett.* **2013**, *13*, 564-569.

(17) Tan, S. F.; Wu, L.; Yang, J. K. W.; Bai, P.; Bosman, M.; Nijhuis, C. A. Quantum Plasmon Resonances Controlled by Molecular Tunnel Junctions. *Science* **2014**, *343*, 1496-1499.

(18) Zhu, W.; Crozier, K. B. Quantum Mechanical Limit to Plasmonic Enhancement as Observed by Surface-Enhanced Raman Scattering. *Nature Comm.* **2014**, *5*, 5228.

(19) Toscano, G.; Rockstuhl, C.; Evers, F.; Xu, H.; Mortensen, N. A. Self-consistent Hydrodynamic Approach to Nanoplasmonics: Resonance Shifts and Spill-out effects. *arXiv:*1048:5862 preprint.

(20) Esteban, R.; Borisov, A. G.; Nordlander, P.; Aizpurua, J. Bridging Quantum and Classical Plasmonics with a Quantum-Corrected Model. *Nature Comm.* **2012**, *3*, 825.

(21) Atay, T.; Song, J.-H.; Nurmikko, A. V. Strongly Interacting Plasmon Nanoparticle Pairs: From Dipole-Dipole Interaction to Conductively Coupled Regime. *Nano Lett.* **2004**, *4*, 1627-1631.

(22) Marhaba, S.; Bachelier, G.; Bonnet, C.; Broyer, M.; Cottancin, E.; Grillet, N.; Lermé, J.; Vialle, J.-L.; Pellarin, M. Surface Plasmon Resonance of Single Gold Nanodimers near the Conductive Contact Limit. *J. Phys. Chem. C* **2009**, *113*, 4349-4356.

(23) Pérez-González, O.; Zabala, N.; Borisov, A. G.; Halas, N. J.; Nordlander, P. Optical Spectroscopy of Conductive Junctions in Plasmonic Cavities. *Nano Lett.* **2010**, *10*, 3090-3095.

(24) Zuloaga, J.; Prodan, E.; Nordlander, P. Quantum Description of the Plasmon Resonances of a Nanoparticle Dimer. *Nano Lett.* **2009**, *9*, 887-891.

(25) Marinica, D. C.; Kazansky, A. K.; Nordlander, P.; Aizpurua, J.; Borisov, A. G. Quantum Plasmonics: Nonlinear Effects in the Field Enhancement of a Plasmonic Nanoparticle Dimer. *Nano Lett.* **2012**, *12*, 1333-1339.

(26) Runge, E.; Gross, E. K. U. Density-Functional Theory for Time-Dependent Systems. *Phys. Rev. Lett.* **1984**, *52*, 997-1000.

(27) Onida, G.; Reining, L.; Rubio, A. Electronic Excitations: Density-Functional Versus Many-Body Green's-Function Approaches. *Rev. Mod. Phys.* **2002**, *74*, 601-659.

(28) Pitarke, J. M.; Silkin, V. M.; Chulkov, E. V.; Echenique, P. M. Theory of Surface Plasmons and Surface-Plasmon Polaritons. *Rep. Prog. Phys.* **2007**, *70*, 1-87.

(29) Marques, M. A. L.; Maitra, N. T.; Nogueira, F. M. S.; Gross, E. K. U.; Rubio, A. (Eds.) *Fundamentals of Time-Dependent Density Functional Theory*, Springer: Berlin, **2012**.

(30) Zuloaga, J.; Prodan, E.; Nordlander, P. Optical Properties and Tunability of Metallic Nanorods. *ACS Nano* **2010**, *4*, 5269-5276.

(31) Stella, L.; Zhang, P.; García-Vidal, F. J.; Rubio, A.; García-González, P. Performance of Nonlocal Optics when Applied to Plasmonic Nanostructures. *J. Phys. Chem. C*, **2013** *117*, 8941-8949.

(32) Teperik, T. V.; Nordlander, P.; Aizpurua, J.; Borisov, A. G. Robust Subnanometric Plasmon Ruler by Rescaling of the Nonlocal Optical Response. *Phys. Rev. Lett.* **2013**, *110*, 263901.

(33) Teperik, T. V.; Nordlander, P.; Aizpurua, J.; Borisov, A. G. Quantum Effects and nonlocality in Strongly Coupled Plasmonic Nanowire Dimers. *Opt. Express* **2013**, *21*, 27306-27325.

(34) Andersen, K.; Jensen, K. L.; Mortensen, N. A.; Thygesen, K. S. Visualizing Hybridized Quantum Plasmons in Coupled Nanowires: From Classical to Tunneling Regime. *Phys. Rev. B* **2013**, *87*, 235433.

(35) Kulkarni, V.; Prodan, E.; Nordlander, P. Quantum Plasmonics: Optical Properties of a Nanomatryushka. *Nano Lett.* **2013**, *13*, 5873-5879.

(36) Zhang, H.; Kulkarni, V.; Prodan, E.; Nordlander, P.; Gorovov, O. Theory of Quantum Plasmon Resonances in Doped Seminconductor Nanocrystals. *J. Phys. Chem. C* **2014**, *118*, 16035-16042.

(37) McMahon, J. M.; Gray, S. K.; Schatz, G. C. Nonlocal Optical Response of Metal Nanostructures with Arbitrary Shape. *Phys. Rev. Lett.* **2009**, *103*, 097403.

(38) McMahon, J. M.; Gray, S. K.; Schatz, G. C. Optical Properties of Nanowire Dimers with a Spatially Nonlocal Dielectric Function. *Nano Lett.* **2010**, *10*, 3473-3481.

(39) David, C.; García de Abajo, F. J. Spatial Nonlocality in the Optical Response of Metal Nanoparticles. *J. Phys. Chem C* **2011**, *115*, 19470-19475.

(40) Raza, S.; Toscano, G.; Jauho, A.-P.; Wubs, M.; Mortensen, N. A. Unusual Resonances in Nanoplasmonic Structures Due to Nonlocal Response. *Phys. Rev. B* **2011**, *84*, 121412(R).

(41) Toscano, G.; Raza, S.; Jauho, A.-P.; Mortensen, N. A.; Wubs, M. Modified Field Enhancement in Plasmonic Nanowire Dimers Due to Nonlocal Response. *Opt. Express* **2012**, *20*, 4176-4188.

(42) Fernández-Domínguez, A. I.; Wiener, A.; García-Vidal, F. J.; Maier, S. A.; Pendry, J. B. Transformation-Optics Description of Nonlocal Effects in Plasmonic Nanostructures. *Phys. Rev. Lett.* **2012**, *108*, 106802.

(43) Fernández-Domínguez, A. I.; Zhang, P.; Luo, Y.; Maier, S. A.; García-Vidal, F. J.; Pendry, J. B. Transformation-Optics Insight into Nonlocal Effects in Separated Nanowires. *Phys. Rev. B* **2012**, *84*, 241110(R).

(44) Dong, T.; Ma, X; Mittra, R. Optical Response in Subnanometer Gaps due to Nonlocal Response and Quantum Tunneling. *Appl. Phys. Lett.* **2012**, *101*, 233111.

(45) Christensen, T.; Yan, W.; Raza, S.; Jauho, A.-P.; Mortensen, N. A.; Wubs, M. Nonlocal Response of Metallic Nanospheres Probed by Light, Electrons, and Atoms. *ACS Nano* **2014**, *8*, 1745-1758.

(46) Liebsch, A. Surface-plasmon Dispersion and Size Dependence of Mie Resonance: Silver versus Simple Metals. *Phys. Rev. B* **1993**, *48*, 11317-11328.

(47) Weissker, H.-Ch.; Barron Escobar, H.; Thanthirige, V. D.; Kwak, K.; Lee, D.; Ramakrishna, G.; Whetten, R. L.; López-Lozano, X. Information on Quantum States Pervades the Visible Spectrum of the Ubiquitous $Au_{144}(SR)_{60}$ Gold Nanocluster. *Nature Communications* **2014**, *5*, 3785.

(48) Zhang, P.; Feist, J.; Rubio, A.; García-González, P.; García-Vidal, F. J. Ab initio Nanoplasmonics: The impact of atomic structure. *Phys. Rev. B*, **2014**, *90*, 161407(R).

(49) Noya, E. G.; Doye, J. P. K.; Wales, D. J.; Aguado, A. Geometric Magic Numbers of Sodium Clusters: Interpretation of the Melting Behaviour. *Eur. Phys. J. D* **2007**, *43*, 57-60.

(50) The relaxed atomic structure of the Na_{297} cluster is taken from the Cambridge Cluster Database, `http://www-wales.ch.cam.ac.uk/CCD.html`.

(51) Kohn, W.; Sham, L. J. Self-Consistent Equations Including Exchange and Correlation Effects. *Phys. Rev.* **1965**, *140*, A1133-A1138 .

(52) Marques, M. A. L.; Castro, A.; Bertsch, G. F.; Rubio, A. `octopus`: a First-Principles Tool for Excited Electron-Ion Dynamics. *Comput. Phys. Commun.* **2003**, *151*, 60-78.

(53) Castro, A.; Appel, H.; Oliveira, M.; Rozzi, C.A.; Andrade, X.; Lorenzen, F.; Marques, M. A. L.; Gross, E. K. U.; Rubio, A. `octopus`: a Tool for the Application of Time-Dependent Density Functional Theory. *Phys. Stat. Sol. B* **2006**, *243*, 2465-2488.

(54) Andrade, X.; Alberdi-Rodriguez, J.; Strubbe, D.A.; Oliveira, M.J.T.; Nogueira, F.; Castro, A.; Muguerza, J.; Arruabarrena, A.; Louie, S.G.; Aspuru-Guzik, A.; Rubio, A.; Marques, M.A.L. Time-Dependent Density-Functional Theory in Massively Parallel Computer Architectures: the octopus Project. *J. Phys.: Condens. Matter* **2012**, *24*, 233202.

(55) Andrade, X.; Strubbe, D.; De Giovannini, U.; Larsen, A. H.; Oliveira, M. J. T.; Alberdi-Rodriguez, J.; Varas, A.; Theophilou, I.; Helbig, N.; Verstraete, M. J.; Stella, L.; Nogueira, F.; Aspuru-Guzik, A.; Castro, A.; Marques, M. A. L.; Rubio, A. Real-space grids and the octopus code as tools for the development of new simulation approaches for electronic systems. *Phys. Chem. Chem. Phys.* **2015**, DOI:10.1039/C5CP00351B,

(56) Troullier, N.; Martins, J. L. Efficient pseudopotentials for plane-wave calculations *Phys. Rev. B* **1991**, *43*, 1993-2006.

(57) Bitzek, E.; Koskinen, P.; Gähler, F.; Moseler, M.; Gumbsch, P. Structural Relaxation Made Simple. *Phys. Rev. Lett.* **2006**, *97*, 170201.

(58) Yabana, K.; Bertsch, G. F. Time-dependent local-density approximation in real time. *Phys. Rev. B* **1996**, *54*, 4484-4487.

(59) Prodan, E.; Radloff, C.; Halas, N. J.; Nordlander, P. A Hybridization Model for the Plasmon Response of Complex Nanostructures. *Science* **2003**, *302*, 419-422.

(60) Nordlander, P.; Oubre, C.; Prodan, E.; Li, K.; Stockman, M. I. Plasmon Hybridization of Nanoparticle Dimers. *Nano Lett.* **2004**, *4*, 899-903.

(61) Romero, I.; Aizpurua, J.; Bryant, G. W.; García de Abajo, F. J. Plasmons in Nearly Touching Metallic Nanoparticles: Singular Response in the Limit of Touching Dimers. *Optics Express* **2006**, *14*, 9988-9999.

(62) Luo, Y.; Lei, D. Y.; Maier, S. A.; Pendry, J. B. Transformation-Optics Description of Plasmonics Nanostructures Containing Blunt Edges/Corners: From Symmetric to Asymmetric Edge Rounding. *ACS Nano* **2012**, *6*, 6492-6506.

(63) Lei, D. Y.; Aubry, A.; Luo, Y.; Maier, S. A.; Pendry, J. B. Plasmonic Interaction between Overlapping Nanowires. *ACS Nano* **2011**, *5*, 597-607.

(64) Townsend, E.; Bryant, G. W. Plasmonic Properties of Metallic Nanoparticles: The Effects of Size Quantization. *Nano Lett.* **2012**, *12*, 429-434

(65) Yannouleas, C.; Vigezzi, E.; Broglia, R. A. Evolution of the Optical Properties of Alkali-Metal Microclusters Towards the Bulk: The Matrix Random-Phase-Approximation Description. *Phys. Rev. B* **1993**, *47*, 9849-9861.

(66) Li, J.-H.; Hayashi, M.; Guo, G.-Y. Plasmonic Excitations in Quantum-Sized Sodium Nanoparticles Studied by Time-Dependent Density Functional Calculations. *Phys. Rev. B* **2013**, *88*, 155437.

(67) Mukherjee, S.; Libisch, F.; Large, N.; Neumann, O.; Brown, L. V.; Cheng, J.; Lassiter, J. B.; Carter, E. A.; Nordlander, P.; Halas, N. J. Hot Electrons Do the Impossible: Plasmon-Induced Dissociation of H_2 on Au. *Nano Lett.* **2013**, *13*, 240-247.

(68) Banerjee, A.; Harbola, M. K. Hydrodynamic Approach to Time-Dependent Density Functional Theory; Response Properties of Metal Clusters. *J. Chem. Phys.* **2000**, *113*, 5614-5623

(69) Xiang, H.; Zhang, X.; Neuhauser, D.; Lu, G. Size-Dependent Plasmonics Resonances from Large-Scale Quantum Simulations. *J. Phys. Chem. Lett.* **2014**, *5*, 1163-1169.